

K-Link: Knowledge-Link Graph from LLMs for Enhanced Representation Learning in Multivariate Time-Series Data

Yucheng Wang
Institute for Infocomm Research
Nanyang Technological University
Singapore

Ruibing Jin
Institute for Infocomm Research
Singapore

Min Wu
Institute for Infocomm Research
Singapore

Xiaoli Li
Institute for Infocomm Research
Nanyang Technological University
Singapore

Lihua Xie
Nanyang Technological University
Singapore

Zhenghua Chen
Institute for Infocomm Research
Singapore

ABSTRACT

Sourced from various sensors and organized chronologically, Multivariate Time-Series (MTS) data involves crucial spatial-temporal dependencies, e.g., correlations among sensors. To capture these dependencies, Graph Neural Networks (GNNs) have emerged as powerful tools, yet their effectiveness is restricted by the quality of graph construction from MTS data. Typically, existing approaches construct graphs solely from MTS signals, which may introduce bias due to a small training dataset and may not accurately represent underlying dependencies. To address this challenge, we propose a novel framework named K-Link, leveraging Large Language Models (LLMs) to encode extensive general knowledge and thereby providing effective solutions to reduce the bias. Leveraging the knowledge embedded in LLMs, such as physical principles, we extract a *Knowledge-Link graph*, capturing vast semantic knowledge of sensors and the linkage of the sensor-level knowledge. To harness the potential of the knowledge-link graph in enhancing the graph derived from MTS data, we propose a graph alignment module, facilitating the transfer of semantic knowledge within the knowledge-link graph into the MTS-derived graph. By doing so, we can improve the graph quality, ensuring effective representation learning with GNNs for MTS data. Extensive experiments demonstrate the efficacy of our approach for superior performance across various MTS-related downstream tasks.

CCS CONCEPTS

• **Computing methodologies** → *Learning paradigms*; • **Mathematics of computing** → *Time series analysis*.

KEYWORDS

Multivariate Time-Series Data, Graph Neural Network, Large Language Models

Permission to make digital or hard copies of all or part of this work for personal or classroom use is granted without fee provided that copies are not made or distributed for profit or commercial advantage and that copies bear this notice and the full citation on the first page. Copyrights for components of this work owned by others than the author(s) must be honored. Abstracting with credit is permitted. To copy otherwise, or republish, to post on servers or to redistribute to lists, requires prior specific permission and/or a fee. Request permissions from permissions@acm.org.
KDD 2024, Aug 25–29, 2024, Barcelona, ESP

© 2018 Copyright held by the owner/author(s). Publication rights licensed to ACM.
ACM ISBN 978-1-4503-XXXX-X/18/06
<https://doi.org/XXXXXXXX.XXXXXXX>

ACM Reference Format:

Yucheng Wang, Ruibing Jin, Min Wu, Xiaoli Li, Lihua Xie, and Zhenghua Chen. 2018. K-Link: Knowledge-Link Graph from LLMs for Enhanced Representation Learning in Multivariate Time-Series Data. In *Proceedings of (KDD 2024)*. ACM, New York, NY, USA, 12 pages. <https://doi.org/XXXXXXXX.XXXXXXX>

1 INTRODUCTION

Multivariate Time-Series (MTS) data has gained prominence across diverse tasks [10, 41, 42]. To achieve optimal performance for these tasks, learning decent representations from MTS data has become a pivotal research focus. Given that MTS data is commonly acquired from various sensors and organized chronologically, the inherent spatial-temporal dependencies manifest in the data, including correlations among sensors and temporal dependencies among timestamps [6, 31]. To generate high-quality representations, it is crucial to recognize these spatial-temporal dependencies. With the development of Deep Learning (DL) technology, massive DL models are proposed to leverage these dependencies for effective representation learning from MTS data.

In the realm of DL models, traditional approaches predominantly employed Convolutional Neural Network (CNN) [9, 19] or Long-Short Term Memory (LSTM) [21, 22] to learn representations for MTS data. However, these models primarily emphasize capturing temporal dependencies and often neglect to effectively leverage spatial dependencies, limiting their performance. To address this challenge, Graph Neural Networks (GNNs) have emerged as promising solutions [6, 11, 18]. Their capability to capture both spatial and temporal dependencies makes GNNs effective in learning superior representations from MTS data compared to conventional models. To leverage GNNs for MTS data, graph construction is typically necessary. Conventionally, prevalent approaches construct graphs by relying solely on the MTS data itself to model spatial-temporal dependencies [12, 34]. However, the constructed graph may be biased by the distribution of a small training dataset, hampering its ability to generalize effectively in complex scenarios. Notably, as the efficacy of GNNs highly relies on the quality of the graphs derived from MTS data, this limitation affects the representation learning of existing GNN-based methods for MTS data.

The above challenge can be alleviated by integrating Large Language Models (LLMs) into the graph construction process. With billions of parameters and trained on extensive real-world data,

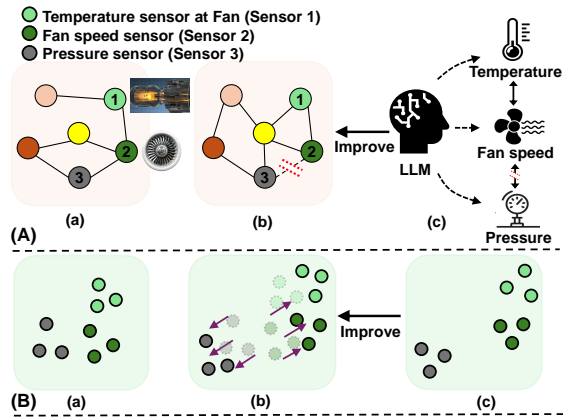


Figure 1: A: (a) The graph derived from MTS signals illustrate correlations among sensors, e.g., connected temperature and fan speed nodes indicating a high correlation between the sensors. However, the graph may be biased by small training datasets, leading to biased connections between fan speed and pressure. (b) The graph is improved by incorporating general knowledge extracted from LLMs, e.g., physical principles in (c). For instance, leveraging the general insight that the fan speed should exhibit a high correlation with the temperature of the fan instead of with the pressure, the edge between fan speed and pressure nodes is removed. B: (a) The bias leads to close feature distributions for sensors. (b) The bias is reduced by incorporating general real-world knowledge in (c).

LLMs can memorize comprehensive general knowledge, demonstrating remarkable generalization capability and providing an effective solution to reduce bias. Using Fig. 1 as an example, the graph derived from MTS data reflects correlations among sensors, such as their physical relations. As shown in Fig. 1 (a), connected temperature and fan speed nodes indicate a high correlation between the two sensors. However, biases introduce connections between fan speed and pressure nodes. Leveraging general physical insights that the fan speed should exhibit a high correlation with the temperature of the fan instead of with the pressure in Fig. 1 (c), the graph can be improved as Fig. 1 (b) by removing biased connections. By leveraging the semantic knowledge of sensors and the underlying physical principles that link the knowledge, the graph quality can be enhanced to effectively represent relationships among sensors.

Adapting LLMs to enhance graph quality involves two key challenges. First, although LLMs store extensive general knowledge, the knowledge is implicitly embedded in numerous parameters. To improve graph construction, it is crucial to explicitly extract the knowledge, including semantic knowledge of sensors and the linkage of the knowledge. Second, adapting the extracted general knowledge to enhance graph quality presents a significant challenge. Despite the wide utilization of LLMs, recent exploration in time-series data [14, 40, 46] has not adequately tackled these challenges. Existing efforts mainly focus on fine-tuning LLMs, but these models are not inherently tailored for graph structures within MTS data. This poses challenges for existing methods in explicitly

extracting sensor-level knowledge and establishing relationships, leading to limitations in guiding the graph construction process.

Motivated by the above challenges, we design a framework based on a *Knowledge-Link graph*, namely K-Link, for MTS data. Our approach comprises two main branches: the signal and knowledge branches. In the signal branch, we follow prior works [34] and construct a graph to capture spatial-temporal dependencies within MTS data. Considering that graphs derived solely from MTS signals may be biased and not accurately represent dependencies, we introduce LLMs to improve the graph quality. In the knowledge branch, we extract a knowledge-link graph with the general knowledge embedded within LLMs, explicitly representing the semantic knowledge of sensors and the linkage of sensor-level knowledge. To effectively leverage the knowledge-link graph, a graph alignment module is proposed, aiming to transfer the semantic knowledge within the knowledge-link graph into the graph derived from MTS data for improved graph quality. This module encompasses two key components, node and edge alignment, with the objective of aligning sensors and their relations between two branches. Through this process, we can enhance the quality of the MTS-derived graph, leading to improved representation learning for MTS data.

Our contributions are three points. First, to mitigate the bias introduced by small training datasets, we introduce a knowledge-link graph. This graph, extracted from LLMs, includes nodes and edges that represent vast semantic knowledge of sensors and the linkage of sensor-level knowledge, providing solutions to reduce bias. Second, to effectively utilize the knowledge-link graph in improving graph quality, we propose a graph alignment module to transfer semantic knowledge of the knowledge-link graph into MTS-derived graph. This module consists of two essential components, node and edge alignment, to align sensors and their relations across two branches. Third, we conduct comprehensive experiments to demonstrate the efficacy of our approach, K-Link, for improved performance across various MTS-related downstream tasks.

2 RELATED WORK

2.1 MTS Representation Learning with GNNs

Due to the inherent temporal ordering of MTS data, traditional methods predominantly emphasized capturing temporal dependencies among timestamps. To learn representations, these works mainly employed CNN [8, 9, 19, 30, 32, 44], LSTM [7, 21, 22], and Transformers [36, 43, 45]. However, MTS data is typically collected from multiple sensors, and these approaches often overlooked the crucial spatial dependencies among sensors, consequently restricting their performance of learning representations for MTS data. To address this problem, GNNs, capable of capturing both the spatial-temporal dependencies, have emerged as effective solutions, demonstrating better performance than traditional methods [13]. Since MTS data inherently lacks explicit graphs, graph construction is normally required before GNNs. To construct graphs, current works [11, 17, 32, 34] mainly employed encoders to learn features for each sensor, with which graphs can be constructed. For example, Hier-CorrPool [32] adopted CNN to extract features, which were used to construct sequential graphs with similarities among sensors. HAGCN [17] employed LSTM to extract temporal features, which were then used to construct graphs that were further processed by

GNN. However, these methods rely solely on MTS signals for graph construction, which may be biased by the distributions of a small training dataset. This limitation hampers effective generalization in complex scenarios, impacting graph quality and, consequently, the representation learning capabilities of GNNs for MTS data.

2.2 LLMs for Time-Series Data

In recent years, the rise of LLMs has marked a paradigm shift, establishing them as a powerful complement to DL models. With the capability to memorize extensive general knowledge through billions of parameters, LLMs encapsulate the vast semantic knowledge of sensors and the underlying relations of the knowledge, offering a promising solution to reduce the bias within the graph solely derived from MTS data and thus improving the graph quality.

Currently, researchers have embarked on exploring the potential of LLMs for time-series data [3, 14, 27, 40, 46]. PromptCast [40] was the pioneering effort to introduce LLMs into the time-series forecasting task by translating numerical signals into prompts. TIME-LLM [14] reimagined LLMs for general time-series forecasting by reformulating time-series data into text prototypes that align naturally with LLMs' capabilities. LLM4TS [3] proposed a two-stage fine-tuning approach tailored for time-series forecasting, aligning LLMs with the characteristics of time-series data to adapt pre-trained models for time-series representations. TEST [27] integrated text prompts with time-series encoding to enhance the alignment of time-series data with natural language. OFA [46] achieved fine-tuning by modifying specific layers of a pre-trained LLM for time-series data analytics. While existing efforts have made significant strides in applying LLMs to time-series data, they face challenges when dealing with MTS data, as discussed earlier. The current works predominantly focus on fine-tuning LLMs without adapting them specifically for the graph structure within MTS data. Consequently, these efforts fall short in explicitly extracting general knowledge of sensors and the linkage of these sensor-level knowledge, limiting their capacity to guide the graph construction for MTS data.

3 METHODOLOGY

3.1 Problem Definition

In a dataset \mathcal{D} comprising n labeled MTS samples denoted as $\{X_a, y_a\}_{a=1}^n$, each sample $X_a \in \mathbb{R}^{N \times L}$ is derived from N sensors with L timestamps. To model the spatial-temporal dependencies within each sample X_a , we construct a graph $G_a = \{V_a, E_a\}$, where nodes V_a with features Z_a denote sensors and edges E_a represent correlations among these sensors. This graph can then be processed by GNN, allowing us to effectively leverage the dependencies to learn effective representations for MTS samples. The subscript a is omitted for simplicity in the following parts.

3.2 Overall Structure

To enhance the graph quality and facilitate improved representation learning with GNNs, we propose a framework that incorporates knowledge within LLMs. Our framework consists of two branches: the signal and knowledge branches. In the signal branch, sensor features are learned using encoders and then utilized for graph construction. The graph derived from MTS data is processed by GNN to capture spatial-temporal dependencies. To improve the

graph quality, we introduce a knowledge-link graph by extracting general knowledge from LLMs in the knowledge branch. Recognizing the effectiveness of prompts in unlocking LLMs' potential [24], sensor-level prompts are designed for extracting sensor semantic knowledge, and label-level prompts are further introduced to consider potential variations in sensor knowledge across distinct categories. To link the sensor-level knowledge, we generate a graph by establishing edges between them. With the knowledge-link graph which captures semantic knowledge of sensors and their relationships, we then introduce a graph alignment module to improve the graph derived from MTS signals. The module comprises node and edge alignment, aiming to align nodes and edges between the MTS-derived graph and the knowledge-link graph. Finally, a readout function is employed to obtain final features for downstream tasks.

3.3 Signal branch

We begin by constructing a graph for MTS data. Traditional graph construction methods [6, 33] typically construct separate graphs for each timestamp. However, these approaches neglect correlations between different sensors at different timestamps [34], failing to fully capture spatial-temporal dependencies within MTS data. To tackle this issue, we construct a fully-connected graph for each MTS sample by following prior work [34]. The process involves sample partition, graph construction, and graph convolution.

Sample Partition: Recognizing local temporal properties of MTS data [32], we partition a sample $X \in \mathbb{R}^{N \times L}$ into distinct patches. Specifying a patch size f , we obtain a set of patches $\{X_t\}_{t=1}^{\hat{L}}$ from X , where each patch is represented as $X_t = \{x_{t,i}\}_{i=1}^N \in \mathbb{R}^{N \times f}$, with $x_{t,i} \in \mathbb{R}^f$. t is the patch index denoted as a timestamp, and \hat{L} represents the quantity of patches, calculated as $\hat{L} = \lfloor \frac{L}{f} \rfloor$ with $\lfloor \cdot \rfloor$ denoting truncation. In each patch, an encoder $f_c(\cdot|W_c)$ works at the sensor level, learning sensor features $x'_{t,i} = f_c(x_{t,i}|W_c)$.

Graph Construction: With the learned sensor features, we proceed to construct a fully-connected graph that interconnects all sensors across all patches. First, we define the nodes of the graph. We totally have N sensors across \hat{L} patches, which leads to $(N\hat{L})$ nodes with features $\{X'_1, \dots, X'_{N\hat{L}}\} = \{x'_{1,1}, \dots, x'_{1,N}, \dots, x'_{\hat{L},1}, \dots, x'_{\hat{L},N}\}$. For simplicity, we denote Z^S as node features, where $z_1^S = x'_{1,1}$, $z_N^S = x'_{1,N}$, $z_{N(\hat{L}-1)+1}^S = x'_{\hat{L},1}$, $z_{(N\hat{L})}^S = x'_{\hat{L},N}$. Then, we have the node set $V^S = \{v_i^S\}_i^{(N\hat{L})}$ with node features $Z^S = \{z_i^S\}_i^{(N\hat{L})}$. Subsequently, we establish the edges of the graph, which are defined by similarities among node features [31]. Here, the dot product is employed to compute the similarities as $e_{ij}^S = f_s(z_i^S)(f_s(z_j^S))^T$, $i, j \in [1, (N\hat{L})]$, with $f_s(z) = zW_s$ to enhance the expressive capacity [29, 34]. The softmax function is then utilized to normalize the edges. Finally, we derive the graph $G^S = (Z^S, E^S)$, where $V^S = \{v_i^S\}_i^{(N\hat{L})}$ with node features $Z^S = \{z_i^S\}_i^{(N\hat{L})}$, and $E^S = \{e_{ij}^S\}_{i,j=1}^{(N\hat{L})}$.

GNN: We employed the Message Passing Neural Network (MPNN), a variant of GNN, to capture the spatial-temporal dependencies within the graph. Consistent with prior work [34], we incorporate moving windows and temporal pooling to address local spatial-temporal dependencies. Employing moving windows of size M , we

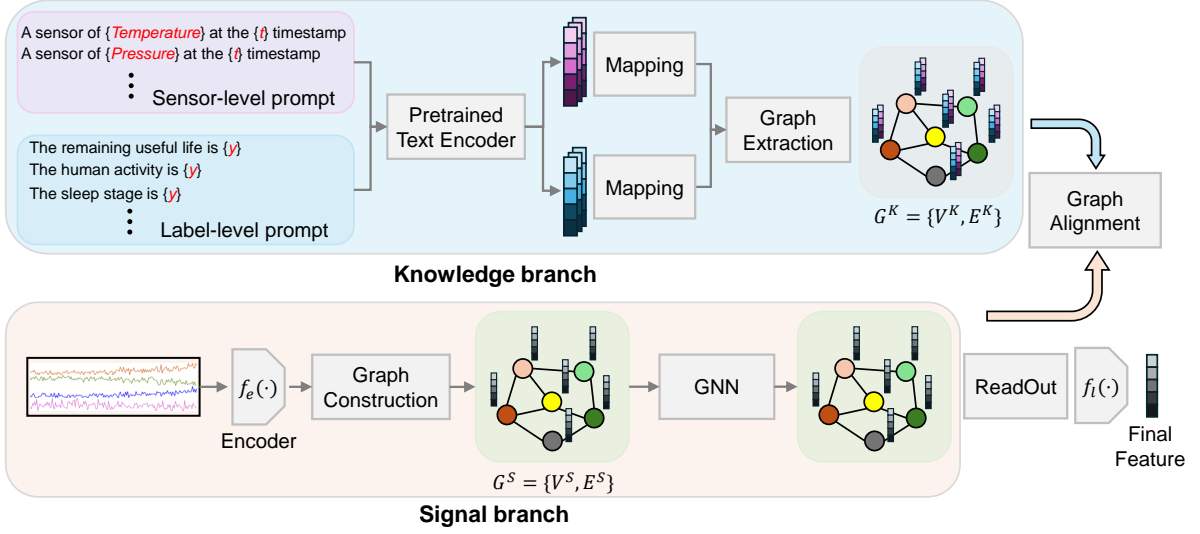


Figure 2: The overall framework. In the signal branch, sensor features are learned using encoders and utilized for graph construction. The graph derived from MTS signals is processed by GNN to capture spatial-temporal dependencies. In the knowledge branch, we introduce a knowledge-link graph by extracting general knowledge from LLMs. To unlock LLMs’ potential, sensor-level prompts are designed to extract sensor knowledge, and label-level prompts are further designed to describe sensor knowledge in distinct categories. The sensor-level knowledge is utilized to define edges in the graph, forming links between them. We then propose a graph alignment module to leverage the knowledge-link graph for better graph quality.

generate sub-graphs by traversing along patches with one step at a time. For the $(m + 1)$ -th window, the sub-graph encapsulate nodes $V_{m+1}^S = \{v_i^S\}_{i=(mN+1)}^{(m+M)N}$ and corresponding edges, e.g., $V_1^S = \{v_i^S\}_{i=1}^{2N}$ for the 1-st window with $M = 2$. Subsequently, MPNN is adopted for the sub-graph in each window. MPNN comprises propagation and updating stages. For a node z_i^S , it has neighboring nodes $\{z_j^S\}_{j \in \mathcal{N}(i)}$ in the same window, and the correlations with its neighbors are represented as $\{e_{ij}^S\}_{j \in \mathcal{N}(i)}$. In the propagation stage, features from neighboring nodes are transmitted into the central node and aggregated with their corresponding edge weights, generating aggregated features $h_i = \sum_{j \in \mathcal{N}(i)} z_j^S e_{ij}^S$. Subsequently, in the updating stage, a non-linear function is utilized to update the aggregated sensor features, resulting in $z_i^{S'} = f_g(h_i | W_g)$. Updated node features are concatenated using a readout function as $D = [z_1^{S'} | \dots | z_{(NL)}^{S'}]$, which can be mapped with a function $f_l(\cdot)$ for downstream tasks.

3.4 Knowledge branch

Equipped with billions of trainable parameters and trained on extensive real-world knowledge, LLMs store vast general knowledge that can enhance graph quality. For instance, the knowledge about physical principles serve as guidance for sensors’ relations. To leverage the potential of LLMs for improved graph construction, we extract a knowledge-link graph, aiming to represent sensor semantic knowledge and the linkage of the sensor-level knowledge.

3.4.1 Knowledge-link graph extraction. To extract a knowledge-link graph from LLMs, three points need to be required.

- The graph should adhere to the fundamental structure of a graph, comprising nodes and edges;

- The graph should be derived from the general knowledge embedded within LLMs.
- The graph should be capable of representing semantic knowledge of each sensor and linking the sensor-level knowledge.

To fulfill the first criteria, we define a graph $G^K = \{V^K, E^K\}$, where V^K and E^K represent nodes and edges, respectively. We aim to extract general knowledge embedded within LLMs to define these nodes and edges. Leveraging LLMs (i.e., point 2), prompts serve as effective tools to unlock their full potential [14, 24, 40, 46]. Hence, sensor- and label-level prompts are designed to extract the general knowledge of each sensor from LLMs, defining nodes in the graph. Then, the edges are determined by the relations of the sensor-level knowledge. By doing so, the nodes represent the semantic knowledge of sensors, and the edges represent the linkage of the sensor-level knowledge, meeting the third point. We elaborate on the details in the subsequent parts.

Sensor-level Prompts: For nodes, we propose designing sensor-level prompts to derive sensor knowledge from LLMs. The prompts should encompass both contextual and sensor-specific information. To meet this requirement, we design prompts ‘A sensor of $[S]$ ’, where ‘sensor’ provides contextual information and $[S]$ represents the sensor name, indicating sensor-specific information. Additionally, considering the temporal properties of MTS data, we extend the sensor-level prompts by incorporating temporal information. The extended prompts take the form of $p_{i,t}$ as ‘A sensor of $[S_i]$ at the $[t]$ timestamp’, where S_i is the name of sensor i , and t corresponds to the t -th timestamp, signifying the t -th patch for this work. By designing sensor-level prompts for all sensors across all patches, we obtain prompts $\{\{p_{i,t}\}_i^N\}_t^L$ for each sample.

Label-level Prompts: Recognizing that samples belonging to different categories may exhibit distinct trends in sensor relations, we design label-level prompts. Taking the example of predicting the Remaining Useful Life (RUL) of a machine, during the degradation stage, the temperature may show a stronger correlation with the fan speed compared to the health stage. This is because the fan in degradation may generate more heat due to increased friction. To account for such category-specific information, we introduce label-level prompts to complement sensor-level prompts. The label-level prompt is defined for each sample, designed as P ‘The [category] is [y]’, where y is the training sample’s label. Notably, [category] may vary depending on specific applications, e.g., ‘The human activity is [y]’ for Human Activity Recognition (HAR) or ‘The remaining useful life of a machine is [y]’ for RUL prediction. With the incorporation of the label-level prompt, we can enhance the sensor-level prompts to capture category-specific sensor relations.

Nodes: With the sensor-level and label-level prompts, we can generate node features for the knowledge-link graph. To achieve this, we leverage the pre-trained text encoder [24] of LLMs. These encoders are trained on extensive real-world data, allowing them to encapsulate rich general knowledge. By utilizing these encoders, we can extract semantic features from LLMs for the nodes in our knowledge-link graph. Specifically, with the encoder \mathcal{F}^K , we derive the sensor-level prompt features $p'_{i,t} = [\mathcal{F}^K(p_{i,t})|\mathcal{F}^K(P)]$. Simplifying the node features in a manner similar to the graph in the signal branch, we define the nodes of the knowledge-link graph as $V^K = \{v_i^K\}_i^{(NL)}$, with node features $Z^K = \{z_i^K\}_i^{(NL)}$, where $z_{N(\hat{L}-1)+1}^K = p'_{\hat{L},1}$, $z_{(NL)}^K = p'_{\hat{L},N}$.

Edges: The edges of the knowledge-link graph should be determined by sensor-level knowledge. For example, the temperature sensor at a fan should be more correlated with the speed sensor of the fan, than with a pressure sensor. To quantify these relations, values should be assigned based on the strength of the relations. Larger values are assigned to sensors with stronger relations, while smaller values are given to those with weaker connections. We calculate these values using similarities among sensor-level prompt features, where high similarity indicates robust semantic links of the sensor-level knowledge. Here, we adopt dot-product for similarity computation, i.e., $e_{ij}^K = z_i^K(z_j^K)^T$. With this approach, we obtain the knowledge-link graph $G^K = (Z^K, E^K)$, where $V^K = \{v_i^K\}_i^{(NL)}$ represents nodes with features $Z^K = \{z_i^K\}_i^{(NL)}$, signifying the semantic features of sensor-level knowledge, and $E^K = \{e_{ij}^K\}_{i,j=1}^{(NL)}$ represents edges, denoting the strength of connections in the sensor-level knowledge. The knowledge-link graph can then be employed to enhance the quality of the graph solely derived from MTS signals.

3.4.2 Graph Alignment. The knowledge-link graph, derived from LLMs trained on extensive data and containing vast general knowledge, is more stable and enriched with semantic knowledge compared to graphs derived solely from MTS signals. Hence, it is useful to transfer the semantic knowledge embedded within the knowledge-link graph into the MTS-derived graph. To do so, we propose a graph alignment module, aiming to align the MTS-derived graph with the knowledge-link graph for improved graph quality. This alignment is facilitated through node and edge alignment,

ensuring that the nodes and edges of the MTS-derived graph are aligned with the knowledge-link graph, as shown in Fig. 3.

Node Alignment: The node features of the knowledge-link graph originate from two sources: sensor-level and label-level prompts, offering semantic knowledge of sensors and categories, respectively. While directly utilizing the whole node features for alignment is simple and intuitive, it may pose challenges in achieving a balanced transfer of sensor-level and label-level semantic knowledge. To address this, we propose to separate node alignment into sensor-level and label-level alignment. This approach allows us to achieve a better balance between two levels and ensure effective transfer of the node semantic knowledge within our knowledge-link graph.

Sensor-level alignment is achieved within each MTS sample. We expect to align corresponding sensors across two branches, distinguishing them from other sensors. This alignment ensures that the features derived from sensor signals are aligned with the sensor’s semantic knowledge. To achieve this, we follow the principles of contrastive learning [35], employing the InfoNCE loss, as shown in Eq. (1), to formulate the sensor-level alignment. \hat{V}_i represents the set of nodes excluding node i . $f_{sim}(\cdot|\cdot)$ is to measure similarity, implemented by the dot product, and τ is a temperature parameter.

$$\mathcal{L}_S = -\frac{1}{(NL)} \sum_i \log \frac{\exp(f_{sim}(z_i^S, z_i^K)/\tau)}{\sum_{v \in \hat{V}_i} \exp(f_{sim}(z_i^S, z_v^K)/\tau)}. \quad (1)$$

Label-level alignment is achieved within each training batch, as the label-level prompt is specified for each sample. We expect to align corresponding samples across two branches, distinguishing them from others. To obtain the features for each sample, we employ a readout function by stacking all sensor features as $g^S = [z_1^S | \dots | z_{(NL)}^S]$. Subsequently, the InfoNCE loss is utilized to achieve the label-level alignment, as shown in Eq. (2). \hat{U}_a denotes the set of samples excluding sample a , and B is the batch size.

$$\mathcal{L}_L = -\frac{1}{B} \sum_{a=1}^B \log \frac{\exp(f_{sim}(g_a^S, g_a^K)/\tau)}{\sum_{u \in \hat{U}_a} \exp(f_{sim}(g_a^S, g_u^K)/\tau)}. \quad (2)$$

Edge Alignment: Edge alignment aims to transfer semantic relations of sensor-level knowledge into sensor correlations derived from MTS signals. To achieve this, we propose to align each edge between two branches, as each edge represents the connection between two sensors. Here, Mean Square Error (MSE) is adopted for the alignment, as shown in Eq. (3).

$$\mathcal{L}_E = \sum_i \sum_j (e_{ij}^S - e_{ij}^K)/(NL)^2. \quad (3)$$

With the node and edge alignment, we combine them to work together as shown in Eq. (4). It is important to note that both sensor-level and edge alignment are performed within each sample, so they are denoted as $\mathcal{L}_{a,S}$ and $\mathcal{L}_{a,E}$ for the a -th sample. λ_S , λ_L , and λ_E are hyperparameters to balance these losses. \mathcal{L}_D is the loss determined by downstream tasks, e.g., cross-entropy loss adopted for classification tasks and MSE adopted for prediction tasks.

$$\mathcal{L} = \mathcal{L}_D + \lambda_S \sum_a \mathcal{L}_{a,S} + \lambda_L \mathcal{L}_L + \lambda_E \sum_a \mathcal{L}_{a,E}. \quad (4)$$

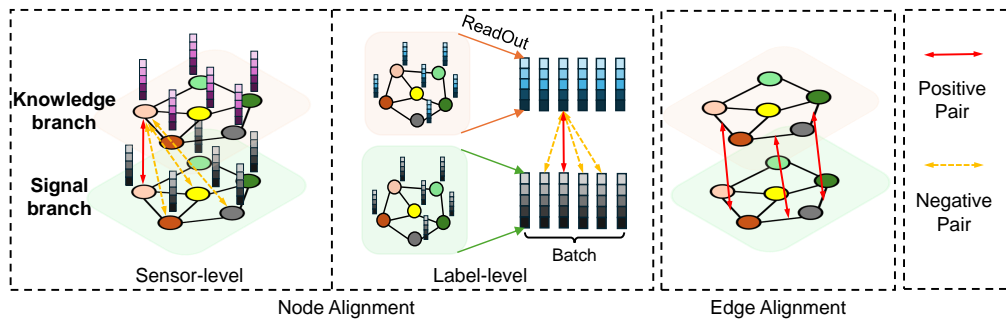


Figure 3: The graph alignment module, comprising node and edge alignment to align nodes and edges between two branches. The node alignment is further divided into sensor- and label-level alignment to strike a better balance between the two levels.

4 EXPERIMENTS

4.1 Experimental Preparations

Datasets: We evaluate our method on three distinct downstream tasks, inspired by previous works [32, 34]: RUL prediction, HAR, and Sleep Stage Classification (SSC). For RUL prediction, we leverage the well-known C-MAPSS dataset [26], specifically adopting the FD002 and FD004 sub-datasets, both of which encompass more complex working conditions compared to other sub-datasets [5]. To maintain consistency with prior studies [32, 34], we utilize the train-test splits provided by the dataset. The training dataset is further partitioned into 80% for training and 20% for validation. Regarding HAR and SSC, we adopted UCI-HAR [2] and ISRUC-S3 [15], where we randomly split these datasets into 60% for training, 20% for validation, and 20% for testing. Further details about these datasets are available in our appendix.

Evaluation: When assessing the performance of RUL prediction, we adopt the Root MSE (RMSE) and the Score function (Score) [5, 33]. Lower values for these metrics signify improved model performance. It is crucial to highlight the significance of Score over RMSE. This preference arises from the fact that Score imposes a more substantial penalty on late predictions, and delayed RUL predictions often result in severe consequences [38]. In evaluating HAR and SSC, we employ Accuracy (Accu.) and Macro-averaged F1-Score (MF1) as performance indicators [8, 23]. Larger values for these metrics denote superior performance.

Implementations: To mitigate the impact of randomness, we conducted each experiment ten times and calculated the average results for analysis. Additionally, we reported standard deviations to demonstrate a model’s robustness. All models are conducted with NVIDIA GeForce RTX 3080Ti and implemented by PyTorch 1.9. Further details about implementations are available in our appendix.

4.2 Comparisons with SOTAs

We benchmark our method against state-of-the-art approaches (SOTAs), including conventional methods that mainly focus on temporal dependencies, such as AConvLSTM [37], DAGN [16], InFormer [45], and AutoFormer [36], as well as GNN-based approaches including HAGCN [17], HierCorrPool [32], MAGNN [4] and FC-STGNN [34]. We directly adopted all results from the comprehensive comparison provided in the previous study [34], aligning with their experimental setting for fair comparisons.

Table 1 showcases the superior performance of our method compared to SOTAs. Notably, GNN-based methods consistently outperform conventional approaches, emphasizing the effectiveness of leveraging spatial dependencies in addition to temporal dependencies for representation learning of MTS data. For RUL prediction, our method outperforms existing GNN-based methods, specifically HierCorrPool on FD002 and FC-STGNN on FD004, both of which are the second-best among SOTAs. Using Score as an evaluation metric, our method demonstrates notable improvements of 10.5% and 3.67% on FD002 and FD004, respectively. Furthermore, our method exhibits the least standard deviation, highlighting its robust performance. Similar enhancements are observed on UCI-HAR and ISRUC-S3, where our method achieves the best performance for these cases. These results underscore the effectiveness of our method, leveraging LLMs to construct superior graphs that capture intricate dependencies within MTS data. This enhancement contributes to the overall improved performance compared to SOTAs.

4.3 Ablation Study

The ablation study is conducted to show the effectiveness of each module. The first variant, labeled ‘w/o knowledge-link’, involves the removal of the knowledge-link graph, utilizing only the signal branch for representation learning. The subsequent category involves the effects of the variations in node alignment during the alignment process. The second variant, ‘w/o node’, eliminates the entire node alignment module. The third variant ‘w/o node (sensor)’ and the fourth variant ‘w/o node (label)’ evaluate the effects of removing sensor-level and label-level alignment, respectively, while retaining another alignment component. Moving to the next category, we explore the effect of removing edge alignment, introducing the fifth variant, ‘w/o edge’. The final variant, ‘w/ index prompt’, employs prompts like ‘A sensor of [index]’, replacing sensor names with numbers (1, 2, etc.), to investigate the utility of sensor semantic knowledge introduced by sensor names.

Table 2 presents the results of the ablation study. We utilize the Score results on FD002 as an example for following analysis. Comparing our complete method with the ‘w/o knowledge-link’ variant, we observe a significant improvement of 21.1%, indicating the effectiveness of the knowledge-link graph extracted from LLMs in enhancing the graph quality. A better graph contributes to improved representations for downstream tasks. Examining the

Table 1: Comparisons with SOTAs (Our method achieves the best compared with SOTAs, including GNNs).

Variants	FD002		FD004		UCI-HAR		ISRUC-S3	
	RMSE	Score	RMSE	Score	Accu.	MF1	Accu.	MF1
AConvLSTM	13.11±0.21	737±65	14.64±0.31	1011±107	86.06±1.01	85.75±1.01	72.93±0.62	69.52±1.00
DAGN	16.43±0.05	1242±116	19.04±0.10	2321±105	89.02±0.49	88.94±0.48	55.35±0.35	50.51±2.78
InFormer	13.20±0.15	715±71	14.16±0.49	1023±201	90.23±0.48	90.23±0.47	72.15±2.41	68.67±3.42
AutoFormer	16.51±0.47	1248±112	20.31±0.14	2291±122	56.70±0.81	54.41±1.74	43.75±0.95	37.88±2.43
HAGCN	14.92±0.12	1086±87	14.66±0.25	880±150	80.79±0.77	81.08±0.75	66.59±0.29	60.20±2.24
HierCorrPool	13.23±0.31	<u>709±61</u>	13.86±0.32	854±68	93.81±0.26	93.79±0.28	79.31±0.60	76.25±0.72
MAGNN	13.09±0.13	714±57	14.30±0.26	978±137	90.91±0.99	90.79±1.08	68.13±2.54	64.31±5.25
FC-STGNN	<u>13.04±0.13</u>	738±49	<u>13.62±0.25</u>	<u>816±63</u>	<u>95.81±0.24</u>	<u>95.82±0.24</u>	<u>80.87±0.21</u>	<u>78.79±0.55</u>
Ours	12.87±0.14	634±30	13.36±0.22	786±61	96.87±0.12	96.92±0.12	81.37±0.20	79.36±0.49

RMSE, Score: Lower is better; Accu., MF1: Higher is better.

Table 2: The ablation study (Performance decreases with removing any modules, indicating their effectiveness).

Variants	FD002		FD004		UCI-HAR		ISRUC-S3	
	RMSE	Score	RMSE	Score	Accu.	MF1	Accu.	MF1
w/o knowledge-link	13.85±0.19	804±91	14.39±0.13	968±56	95.62±0.16	95.64±0.18	79.83±0.14	78.11±0.55
w/o node	13.57±0.25	725±56	14.14±0.19	884±51	96.23±0.12	96.26±0.10	80.19±0.35	78.63±0.66
w/o node (sensor)	13.39±0.10	713±56	14.15±0.30	969±73	96.51±0.09	96.56±0.10	80.42±0.28	78.81±0.49
w/o node (label)	13.36±0.13	712±22	13.94±0.12	881±79	96.35±0.13	96.40±0.13	80.42±0.20	78.72±0.35
w/o edge	13.48±0.05	742±30	13.62±0.09	896±79	96.15±0.12	96.18±0.13	80.10±0.19	78.59±0.59
w/ index prompt	13.30±0.08	702±43	13.76±0.22	867±75	96.49±0.10	96.52±0.11	80.43±0.39	78.70±0.72
Ours	12.87±0.14	634±30	13.36±0.22	786±61	96.87±0.12	96.92±0.12	81.37±0.20	79.36±0.49

RMSE, Score: Lower is better; Accu., MF1: Higher is better.

knowledge-link graph components, both nodes and edges are crucial. Removing node and edge alignment, we observe performance drops of 12.5% and 14.5%, respectively, emphasizing the importance of sensor semantic information and their links in the knowledge-link graph for enhancing MTS-derived graphs’ quality. Within node alignment, the removal of sensor-level and label-level alignment leads to performance decreases of 11.1% and 10.9%, respectively, highlighting the significance of sensor-level and label-level prompts. Finally, replacing sensor names with index numbers results in a 9.68% performance drop, demonstrating the importance of the semantic knowledge within sensor names. Notably, the variant with index prompts achieves slightly better results than the variant without sensor-level alignment, possibly due to the additional contextual information provided by the prompt ‘A sensor of’.

The ablation study underscores the effectiveness of the knowledge-link graph, emphasizing the crucial roles played by both its nodes and edges to represent the general knowledge of sensors and the linkage of the sensor-level knowledge. Derived from the general knowledge within LLMs, the knowledge-link graph significantly enhances the quality of the graph solely derived from MTS signals. This improvement in graph quality translates into better representations learned by GNN, ultimately leading to enhanced overall performance for downstream tasks.

4.4 Sensitivity Analysis

Three hyperparameters, λ_S , λ_L , and λ_E , are introduced to our K-Link, allowing for fine-tuning the impacts of sensor-level, label-level, and edge alignment, respectively. In this section, we analyze their effects by exploring various values within $[0, 1e-5, 1e-4, 1e-3, 1e-2, 1e-1]$, where 0 represents the exclusion of the corresponding loss. The following figures demonstrate their effects, where the left side illustrates the results for RUL prediction, with lower values being preferable, and the right side displays results for HAR and SSC, with higher values being desirable.

Node Alignment Analysis - Sensor: This analysis focuses on the impact of sensor-level prompts, which convey semantic knowledge about individual sensors. The analysis of λ_S depicted in Fig. 4 reveals that a small λ_S , such as $1e-5$, leads to improved performance compared to $\lambda_S = 0$ (i.e., without sensor-level alignment), indicating the effectiveness of sensor-level alignment. However, both too small and large values fail to yield optimal performance. When the value is too small, the sensor-level alignment is insufficient to effectively transfer sensor-level knowledge into the MTS-derived graph. For instance, in the case of Score for FD002 and accuracy for ISRUC-S3, the performance achieved with $\lambda_S = 1e-5$ is worse than the outcomes obtained with $\lambda_S = 1e-4$ or $\lambda_S = 1e-3$. In contrast, large values also result in sub-optimal performance. This occurs because sensor-level prompts encapsulate general semantic knowledge about sensors but do not capture sample-specific details. A

large value of λ_S results in strong sensor-level alignment, where general semantic features dominates over sample-specific features, leading to an excessive loss of sample-specific information and diminished performance. In summary, it is evident that sensor-level prompts contribute positively to performance, but the hyperparameter governing sensor-level alignment should not be too small or too large. $\lambda_S = 1e-4$ or $1e-3$ can help achieve optimal performance.

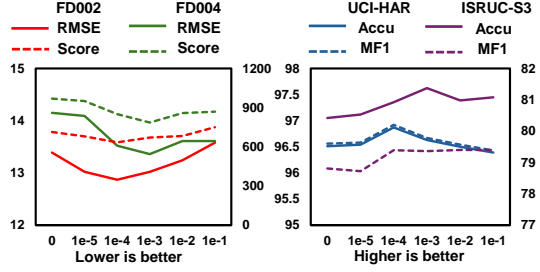


Figure 4: Sensitivity analysis for sensor-level alignment (λ_S).

Node Alignment Analysis - Label: This analysis focuses on the effect of label-level prompts, which provides additional information for variations in different categories. As the analysis of λ_L depicted in Fig. 5, we observe that increasing the value of λ_L enhances performance, underscoring the efficacy of the label-level alignment. However, the performance diminishes with excessively large values. For instance, setting λ_L to $1e-1$ on HAR and SSC fails to yield optimal results. For RUL prediction, the trend stabilizes with λ_L increasing to $1e-2$, and further increases in the value do not yield additional performance gains. Notably, different from λ_S , λ_L attains optimal solutions with relatively larger values, such as $1e-2$ for UCI-HAR, while λ_S achieves optimal performance with relatively smaller values, such as $1e-4$ for UCI-HAR. For this reason, we divide the node alignment into sensor-level and label-level alignment, making it easier to achieve optimal performance.

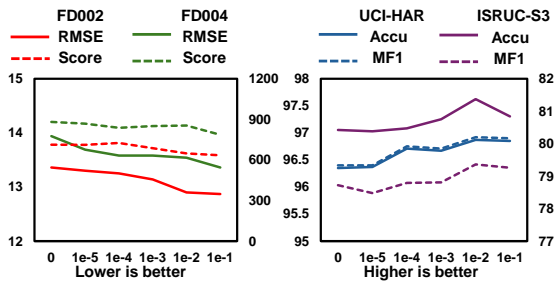


Figure 5: Sensitivity analysis for label-level alignment (λ_L).

Edge Alignment Analysis: This analysis focuses on the effect of edge alignment, which aligns the edges between two graphs to transfer semantic relationships of sensor-level knowledge into sensor correlations derived from MTS signals. Fig. 6 illustrates the analysis of λ_E across different values. From the figure, we observe that even a small value can contribute to better performance than the case of $\lambda_E = 0$, indicating the effectiveness of edge alignment. However, when the value increases to $1e-3$ or $1e-2$, the performance

shows no further improvement and even degrades. This suggests that excessively large λ_E might lead to the excessive loss of relational information among sensors derived from signals. Therefore, $1e-3$ or $1e-2$ can help obtain optimal performance.

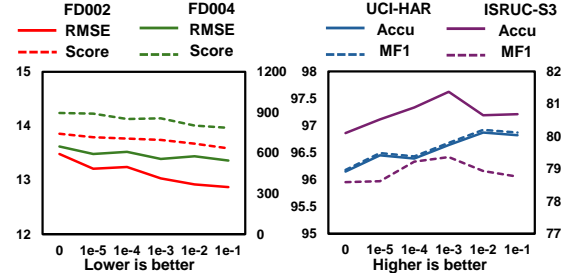


Figure 6: Sensitivity analysis for edge alignment (λ_E).

4.5 Effectiveness of Knowledge-Link Graph

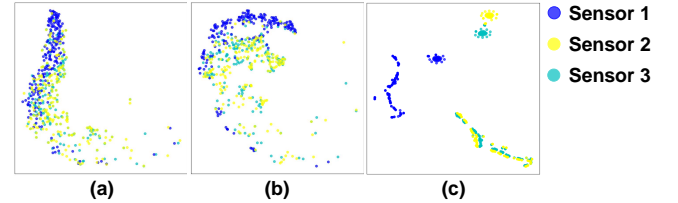


Figure 7: Visualizations. (a) Sensor features derived solely from MTS data. (b) Enhanced sensor features by K-Link. (c) Sensor knowledge extracted from our knowledge-link graph.

To visually demonstrate the effectiveness of our method, we utilize t-SNE [28] to visualize sensor features. For clarity, we select features from three sensors and perform the visualizations using 100 samples from FD002. The results are depicted in Fig. 7, where each point denotes the corresponding sensor for a sample, and proximity between points indicates high correlations.

Fig. 7 (c) presents the feature distributions generated by the general knowledge within our knowledge-link graph. From the figure, we observe that sensors 2 and 3 exhibit close proximity, indicating a high correlation between these sensors, while sensor 1 is distant from the other two sensors, suggesting lower correlations. However, the sensor features derived solely from MTS signals show different distributions in Fig. 7 (a), where feature points for all three sensors are closely clustered, signifying high correlations among them. This inconsistency arises from the bias introduced by small training datasets, leading to biased high correlations between sensor 1 and the other two sensors. The bias impacts the ability to generalize in complex scenarios, affecting graph quality. To address this issue, we leverage the general knowledge encoded in our knowledge-link graph to guide the graph construction. The improved sensor features, as shown in Fig. 7 (b), demonstrate that features from sensor 1 are distinctly separate from the other two sensors. Meanwhile, features from sensors 2 and 3 still exhibit proximity, indicating a maintained correlation. From the visualization, it is evident that

the knowledge-link graph can alleviate biased correlations among sensors, thus improving the quality of the graph solely derived from MTS data. The improved graph can subsequently contribute to the enhanced representation learning of GNN for MTS data.

5 CONCLUSION

When adapting GNNs to MTS data, prevailing methods constructing graphs solely from MTS signals may introduce bias from small training datasets, hindering the ability to effectively capture dependencies within MTS data. To address this challenge, we propose a novel framework named K-Link, leveraging extensive general knowledge embedded within LLMs to reduce the bias. First, we extract a Knowledge-Link graph from LLMs, capturing abundant semantic knowledge of sensors and the linkage of the sensor-level knowledge. Second, to leverage the knowledge-link graph for enhancing the graph derived from MTS data, we propose a graph alignment module comprising node and edge alignment techniques. This module facilitates the transfer of semantic knowledge within the knowledge-link graph to the MTS-derived graph. By doing so, we can improve the graph quality, ensuring effective representation learning with GNNs for MTS data. Extensive experiments demonstrate the efficacy of our approach for superior performance across various MTS-related downstream tasks.

ACKNOWLEDGMENTS

REFERENCES

- Ali Al-Dulaimi, Soheil Zabihi, Amir Asif, and Arash Mohammadi. 2019. Hybrid deep neural network model for remaining useful life estimation. In *ICASSP 2019-2019 IEEE International Conference on Acoustics, Speech and Signal Processing (ICASSP)*. IEEE, 3872–3876.
- Davide Anguita, Alessandro Ghio, Luca Oneto, Xavier Parra, and Jorge L Reyes-Ortiz. 2012. Human activity recognition on smartphones using a multiclass hardware-friendly support vector machine. In *International workshop on ambient assisted living*. Springer, 216–223.
- Ching Chang, Wen-Chih Peng, and Tien-Fu Chen. 2023. Llm4ts: Two-stage fine-tuning for time-series forecasting with pre-trained llms. *arXiv preprint arXiv:2308.08469* (2023).
- Ling Chen, Donghui Chen, Zongjiang Shang, Binqing Wu, Cen Zheng, Bo Wen, and Wei Zhang. 2023. Multi-scale adaptive graph neural network for multivariate time series forecasting. *IEEE Transactions on Knowledge and Data Engineering* (2023).
- Zhenghua Chen, Min Wu, Rui Zhao, Feri Guretno, Ruqiang Yan, and Xiaoli Li. 2020. Machine remaining useful life prediction via an attention-based deep learning approach. *IEEE Transactions on Industrial Electronics* 68, 3 (2020), 2521–2531.
- Ailin Deng and Bryan Hooi. 2021. Graph neural network-based anomaly detection in multivariate time series. In *Proceedings of the AAAI Conference on Artificial Intelligence*, Vol. 35. 4027–4035.
- Shengdong Du, Tianrui Li, Yan Yang, and Shi-Jinn Horng. 2020. Multivariate time series forecasting via attention-based encoder–decoder framework. *Neurocomputing* 388 (2020), 269–279. <https://doi.org/10.1016/j.neucom.2019.12.118>
- Emadelddeen Eldele, Mohamed Ragab, Zhenghua Chen, Min Wu, Chee Keong Kwoh, Xiaoli Li, and Cuntai Guan. 2021. Time-Series Representation Learning via Temporal and Contextual Contrasting. In *Proceedings of the Thirtieth International Joint Conference on Artificial Intelligence, IJCAI-21*. 2352–2359. <https://doi.org/10.24963/ijcai.2021/324>
- Jean-Yves Franceschi, Aymeric Dieuleveut, and Martin Jaggi. 2019. Unsupervised scalable representation learning for multivariate time series. *Advances in neural information processing systems* 32 (2019).
- Ashish Gupta, Hari Prabbhat Gupta, Bhaskar Biswas, and Tanima Dutta. 2020. Approaches and applications of early classification of time series: A review. *IEEE Transactions on Artificial Intelligence* 1, 1 (2020), 47–61.
- Ziyu Jia, Youfang Lin, Jing Wang, Ronghao Zhou, Xiaojun Ning, Yuanlai He, and Yaoshuai Zhao. 2020. GraphSleepNet: Adaptive Spatial-Temporal Graph Convolutional Networks for Sleep Stage Classification.. In *IJCAI* 1324–1330.
- Ziyu Jia, Youfang Lin, Jing Wang, Ronghao Zhou, Xiaojun Ning, Yuanlai He, and Yaoshuai Zhao. 2020. GraphSleepNet: Adaptive Spatial-Temporal Graph Convolutional Networks for Sleep Stage Classification.. In *IJCAI* 1324–1330.
- Ming Jin, Huan Yee Koh, Qingsong Wen, Daniele Zambon, Cesare Alippi, Geoffrey I Webb, Irwin King, and Shirui Pan. 2023. A Survey on Graph Neural Networks for Time Series: Forecasting, Classification, Imputation, and Anomaly Detection. *arXiv preprint arXiv:2307.03759* (2023).
- Ming Jin, Shiyu Wang, Lintao Ma, Zhixuan Chu, James Y Zhang, Xiaoming Shi, Pin-Yu Chen, Yuxuan Liang, Yuan-Fang Li, Shirui Pan, et al. 2023. Time-llm: Time series forecasting by reprogramming large language models. *arXiv preprint arXiv:2310.01728* (2023).
- Sirvan Khalighi, Teresa Sousa, José Moutinho Santos, and Urbano Nunes. 2016. ISRUC-Sleep: A comprehensive public dataset for sleep researchers. *Computer methods and programs in biomedicine* 124 (2016), 180–192.
- Jialin Li, Xueyi Li, and David He. 2019. A Directed Acyclic Graph Network Combined With CNN and LSTM for Remaining Useful Life Prediction. *IEEE Access* 7 (2019), 75464–75475. <https://doi.org/10.1109/ACCESS.2019.2919566>
- Tianfu Li, Zhibin Zhao, Chuang Sun, Ruqiang Yan, and Xuefeng Chen. 2021. Hierarchical attention graph convolutional network to fuse multi-sensor signals for remaining useful life prediction. *Reliability Engineering & System Safety* 215 (2021), 107878.
- Tianfu Li, Zhibin Zhao, Chuang Sun, Ruqiang Yan, and Xuefeng Chen. 2021. Multireceptive Field Graph Convolutional Networks for Machine Fault Diagnosis. *IEEE Transactions on Industrial Electronics* 68, 12 (2021), 12739–12749. <https://doi.org/10.1109/TIE.2020.3040669>
- Chien-Liang Liu, Wen-Hoar Hsaio, and Yao-Chung Tu. 2019. Time Series Classification With Multivariate Convolutional Neural Network. *IEEE Transactions on Industrial Electronics* 66, 6 (2019), 4788–4797. <https://doi.org/10.1109/TIE.2018.2864702>
- Hui Liu, Zhenyu Liu, Weiqiang Jia, and Xianke Lin. 2020. Remaining useful life prediction using a novel feature-attention-based end-to-end approach. *IEEE Transactions on Industrial Informatics* 17, 2 (2020), 1197–1207.
- Yeqi Liu, Chuanyang Gong, Ling Yang, and Yingyi Chen. 2020. DSTP-RNN: A dual-stage two-phase attention-based recurrent neural network for long-term and multivariate time series prediction. *Expert Systems with Applications* 143 (2020), 113082. <https://doi.org/10.1016/j.eswa.2019.113082>
- Bi-Liang Lu, Zhao-Hua Liu, Hua-Liang Wei, Lei Chen, Hongqiang Zhang, and Xiao-Hua Li. 2021. A Deep Adversarial Learning Prognostics Model for Remaining Useful Life Prediction of Rolling Bearing. *IEEE Transactions on Artificial Intelligence* 2, 4 (2021), 329–340. <https://doi.org/10.1109/TAI.2021.3097311>
- Qianwen Meng, Hangwei Qian, Yong Liu, Lizhen Cui, Yonghui Xu, and Zhiqi Shen. 2023. MHCCCL: Masked Hierarchical Cluster-Wise Contrastive Learning for Multivariate Time Series. In *Proceedings of the AAAI Conference on Artificial Intelligence*, Vol. 37. 9153–9161.
- Alec Radford, Jong Wook Kim, Chris Hallacy, Aditya Ramesh, Gabriel Goh, Sandhini Agarwal, Girish Sastry, Amanda Askell, Pamela Mishkin, Jack Clark, et al. 2021. Learning transferable visual models from natural language supervision. In *International conference on machine learning*. PMLR, 8748–8763.
- Alec Radford, Jeffrey Wu, Rewon Child, David Luan, Dario Amodei, Ilya Sutskever, et al. 2019. Language models are unsupervised multitask learners. *OpenAI blog* 1, 8 (2019), 9.
- Abhinav Saxena, Kai Goebel, Don Simon, and Neil Eklund. 2008. Damage propagation modeling for aircraft engine run-to-failure simulation. In *2008 International Conference on Prognostics and Health Management*. 1–9. <https://doi.org/10.1109/PHM.2008.4711414>
- Chenxi Sun, Yaliang Li, Hongyan Li, and Shenda Hong. 2023. TEST: Text prototype aligned embedding to activate LLM’s ability for time series. *arXiv preprint arXiv:2308.08241* (2023).
- Laurens Van der Maaten and Geoffrey Hinton. 2008. Visualizing data using t-SNE. *Journal of machine learning research* 9, 11 (2008).
- Ashish Vaswani, Noam Shazeer, Niki Parmar, Jakob Uszkoreit, Llion Jones, Aidan N Gomez, Łukasz Kaiser, and Illia Polosukhin. 2017. Attention is all you need. *Advances in neural information processing systems* 30 (2017).
- Kang Wang, Kenli Li, Liqian Zhou, Yikun Hu, Zhongyao Cheng, Jing Liu, and Cen Chen. 2019. Multiple convolutional neural networks for multivariate time series prediction. *Neurocomputing* 360 (2019), 107–119. <https://doi.org/10.1016/j.neucom.2019.05.023>
- Yucheng Wang, Min Wu, Ruibing Jin, Xiaoli Li, Lihua Xie, and Zhenghua Chen. 2023. Local-Global Correlation Fusion-Based Graph Neural Network for Remaining Useful Life Prediction. *IEEE Transactions on Neural Networks and Learning Systems* (2023).
- Yucheng Wang, Min Wu, Xiaoli Li, Lihua Xie, and Zhenghua Chen. 2023. Multivariate Time Series Representation Learning via Hierarchical Correlation Pooling Boosted Graph Neural Network. *IEEE Transactions on Artificial Intelligence* (2023).
- Yucheng Wang, Yuecong Xu, Jianfei Yang, Zhenghua Chen, Min Wu, Xiaoli Li, and Lihua Xie. 2023. SEnSOr Alignment for Multivariate Time-Series Unsupervised Domain Adaptation. In *Proceedings of the AAAI Conference on Artificial Intelligence*, Vol. 37. 10253–10261.
- Yucheng Wang, Yuecong Xu, Jianfei Yang, Min Wu, Xiaoli Li, Lihua Xie, and Zhenghua Chen. 2023. Fully-Connected Spatial-Temporal Graph for Multivariate

- Time Series Data. *arXiv preprint arXiv:2309.05305* (2023).
- [35] Yucheng Wang, Yuecong Xu, Jianfei Yang, Min Wu, Xiaoli Li, Lihua Xie, and Zhenghua Chen. 2023. Graph-Aware Contrasting for Multivariate Time Series Classification. *arXiv preprint arXiv:2309.05202* (2023).
- [36] Haixu Wu, Jiehui Xu, Jianmin Wang, and Mingsheng Long. 2021. Autoformer: Decomposition transformers with auto-correlation for long-term series forecasting. *Advances in Neural Information Processing Systems* 34 (2021), 22419–22430.
- [37] Yuteng Xiao, Hongsheng Yin, Yudong Zhang, Honggang Qi, Yundong Zhang, and Zhaoyang Liu. 2021. A dual-stage attention-based Conv-LSTM network for spatio-temporal correlation and multivariate time series prediction. *International Journal of Intelligent Systems* 36, 5 (2021), 2036–2057.
- [38] Qing Xu, Zhenghua Chen, Keyu Wu, Chao Wang, Min Wu, and Xiaoli Li. 2021. KDnet-RUL: A knowledge distillation framework to compress deep neural networks for machine remaining useful life prediction. *IEEE Transactions on Industrial Electronics* 69, 2 (2021), 2022–2032.
- [39] Tiantian Xu, Guangjie Han, Linfeng Gou, Miguel Martínez-García, Dong Shao, Bin Luo, and Zhenyu Yin. 2022. SGBRT: an edge-intelligence based remaining useful life prediction model for aero-engine monitoring system. *IEEE Transactions on Network Science and Engineering* 9, 5 (2022), 3112–3122.
- [40] Hao Xue and Flora D Salim. 2023. Promptcast: A new prompt-based learning paradigm for time series forecasting. *IEEE Transactions on Knowledge and Data Engineering* (2023).
- [41] Jianfei Yang, Yuecong Xu, Haozhi Cao, Han Zou, and Lihua Xie. 2022. Deep learning and transfer learning for device-free human activity recognition: A survey. *Journal of Automation and Intelligence* 1, 1 (2022), 100007.
- [42] Raneen Younis, Zahra Ahmadi, Abdul Hakmeh, and Marco Fisichella. 2023. Flames2graph: An interpretable federated multivariate time series classification framework. In *Proceedings of the 29th ACM SIGKDD Conference on Knowledge Discovery and Data Mining*. 3140–3150.
- [43] George Zerveas, Srideepika Jayaraman, Dhaval Patel, Anuradha Bhamidipaty, and Carsten Eickhoff. 2021. A transformer-based framework for multivariate time series representation learning. In *Proceedings of the 27th ACM SIGKDD conference on knowledge discovery & data mining*. 2114–2124.
- [44] Xuchao Zhang, Yifeng Gao, Jessica Lin, and Chang-Tien Lu. 2020. Tapnet: Multivariate time series classification with attentional prototypical network. In *Proceedings of the AAAI Conference on Artificial Intelligence*, Vol. 34. 6845–6852.
- [45] Haoyi Zhou, Shanghang Zhang, Jieqi Peng, Shuai Zhang, Jianxin Li, Hui Xiong, and Wancai Zhang. 2021. Informer: Beyond efficient transformer for long sequence time-series forecasting. In *Proceedings of the AAAI Conference on Artificial Intelligence*, Vol. 35. 11106–11115.
- [46] Tian Zhou, Peisong Niu, Xue Wang, Liang Sun, and Rong Jin. 2023. One Fits All: Power General Time Series Analysis by Pretrained LM. *arXiv preprint arXiv:2302.11939* (2023).

A DATASET DETAILS

C-MAPSS is employed for the task of remaining useful life prediction. This dataset encompasses four sub-datasets (FD001, FD002, FD003, and FD004), collected under various conditions. Compared to FD001 and FD003, FD002 and FD004 contain samples collected under more fault modes and working conditions, rendering them more complex scenarios [5]. Therefore, FD002 and FD004 are selected for experimental comparisons in RUL prediction. These subsets include data collected from 21 sensors for status detection. Consistent with previous studies [20, 33], we utilize 14 sensors for analysis, as the remaining sensors (i.e., sensors with indices 1, 5, 6, 10, 16, 18, and 19) maintain constant values. Given that C-MAPSS samples capture the whole life cycle of machines, pre-processing is essential. Specifically, a fixed-length time window of size L slides along the signals in steps of $S = 1$ for each sampling event, resulting in samples with dimension $\mathbb{R}^{N \times L}$, where $N = 14$ represents the number of sensors. Here, L represents the time length of each sample, differing based on dataset characteristics. The label, i.e., the RUL, of the a -th sample denoted as $y_a = T - L - a \times S$. The labels are further transformed using piece-wise linear RUL estimation [1, 39].

As a prediction task, RMSE and Score are adopted to measure the performance for RUL prediction. As shown in Eq. (5) and (6), \hat{y}_a is the value of predicted RUL while y_a represents the value of real RUL. n is the number of samples in a dataset. Notably, RMSE quantifies

the error between the predicted and actual RULs, treating both early and late predictions equally. On the other hand, the Score function imposes a higher penalty on late predictions. As late predictions result in more significant losses than early predictions in real-world productions, the Score function is typically deemed more critical than RMSE for evaluation purposes.

$$\text{RMSE} = \sqrt{\frac{\sum_{a=1}^n (\hat{y}_a - y_a)^2}{n}}, \quad (5)$$

$$\text{Score}_a = \begin{cases} e^{-\frac{\hat{y}_a - y_a}{13}} - 1, & \text{if } \hat{y}_a < y_a \\ e^{\frac{\hat{y}_a - y_a}{10}} - 1, & \text{otherwise} \end{cases}$$

$$\text{Score} = \frac{1}{n} \sum_{a=1}^n \text{Score}_a \quad (6)$$

We utilize the **UCI-HAR** dataset for human activity recognition and the **ISRUC-S3** dataset for sleep stage classification. The UCI-HAR dataset encompasses signals from 30 subjects engaged in six activities: walking, walking upstairs, walking downstairs, standing, sitting, and lying down. Nine sensors are employed for detecting these activities. On the other hand, the ISRUC-S3 dataset comprises signals from ten subjects during five sleep stages: wakefulness, N1 stage, N2 stage, N3 stage, and REM, and ten sensors are utilized in this process. To train and evaluate our model, we randomly divide the data into training (60%), validation (20%), and testing (20%) sets. To mitigate the impact of inter-subject variability, the dataset splitting is performed at the subject level. Additionally, prior to training and evaluation, all datasets are subjected to max-min normalization to ensure consistent scaling of the data.

The statistical details of these datasets are displayed in Table 3. It is noted that the original time length of samples in ISRUC-S3 is 3000, which can be computationally expensive for training. Therefore, we down-sample the samples at intervals of ten, reducing the sample time length to 300.

B STRUCTURE DETAILS

In our K-Link framework, we incorporate two branches: the signal branch and the knowledge branch. The pseudo code is shown in Algorithm 1. We begin by introducing the knowledge branch. In this branch, we have designed sensor-level and label-level prompts to extract general knowledge for sensors. To encode these prompts, we adopted the pretrained text encoder of CLIP [24], based on GPT-2 [25]. The output dimension of the text encoder is 512, which is too large for training a model with small MTS training datasets. To address this, we employ two mapping functions $f_M(\cdot)$ with trainable parameters $W_M \in \mathbb{R}^{512 \times d_h}$ to map the high-dimensional features into a low-dimensional feature space. Subsequently, the prompt features from both levels can be utilized for generating edges of our knowledge-link graph and the following graph alignment. During the graph alignment process, we introduce another mapping function $f_m(\cdot)$ with parameters $W_m \in \mathbb{R}^{d_h \times d_h}$ for the graph generated in the signal branch, aiming to enhance the adaptability of the alignment process.

In the signal branch, two main encoders, a CNN and a GNN, are employed to learn sensor features within each patch and capture spatial-temporal dependencies within a graph, respectively. The

Table 3: Dataset details

Datasets	Dataset statistics				
	Training	Validation	Testing	# Sensors	# Time Length
FD002 (C-MAPSS)	32816	8203	259	14	50
FD004 (C-MAPSS)	39239	9809	248	14	50
UCI-HAR	7947	2649	2649	9	128
ISRUC-S3	5149	1712	1712	10	300

Table 4: Structure details

Datasets	Hyperparameter statistics					
	No. Blocks	CNN Blocks Hyper-parameters	Hidden (d_h)	Linear Layer $f_l(\cdot)$	Patch Size f	Batch Size
FD002 (C-MAPSS)	2	[1, 64, 48], with kernel 2	56	[56*14*5,112,112,56,1]	5	300
FD004 (C-MAPSS)	2	[1, 56, 16], with kernel 2	36	[36*14*5,112,112,56,1]	5	300
UCI-HAR	3	[1, 48, 96, 18] with kernel 6	16	[16*9*1,6]	64	100
ISRUC-S3	3	[1, 64, 128, 64] with kernel 5	72	[72*10*2,144,144,72,5]	75	100

Algorithm 1 Pseudocode of K-Link.

```

# X, MTS sample with [N,L], N: number of sensors, L: time length
# y, label of X
# f, patch size
# L_hat, number of patches
# ts_enc, time series encoders, such as CNN or LSTM

# sns_prompt, prompts for N sensors across L_hat times
# lab_prompt, prompt for the label of X
# F_text, pretrained text encoder
# F_M, mapping function with [512, d_h]
# F_l, function to map the features from GNN for downstream tasks

train()

# Step 1: extract node features for signal branch
sig_patch = sample_partition(X, f) # [L_hat, N, f]
sig_feat = ts_enc(sig_patch) # [L_hat, N, d_h]
sig_node_feat = reshape(sig_feat) # [L_hat*N, d_h]

# Step 2: extract node features for knowledge branch
sns_prompt_feat = F_M(F_text(sns_prompt)) # [L_hat, N, d_h]
lab_prompt_feat = F_M(F_text(lab_prompt)) # [d_h]
prompt_feat = concat(sns_prompt_feat, exp_dim(lab_prompt_feat))
knowl_node_feat = reshape(prompt_feat) # [L_hat*N, 2*d_h]

# Step 3: compute edges for signal and knowledge branches
sig_edge = sig_edge_comp(sig_node_feat) # [L_hat*N, L_hat*N]
knowl_edge = knowl_edge_comp(knowl_node_feat) # [L_hat*N, L_hat*N]

# Step 4: compute losses for graph alignment
loss_sns = sns_level_align(sig_node_feat, reshape(sns_prompt_feat))
loss_lab = lab_level_align(readout(sig_node_feat), sns_prompt_feat)
loss_edge = edge_align(sig_edge, knowl_edge)

# Step 5: compute downstream task loss
loss_D = loss_comp(F_l(MPNN(sig_node_feat, sig_edge)), y)

# Step 6: Derive overall loss and update model parameters
loss = loss_D + lamb_s*loss_sns + lamb_L*loss_lab + lamb_e*loss_edge

loss.backward()
optim.step()

```

CNN-based encoder $f_c(\cdot|W_c)$ comprises several CNN blocks to extract sensor-level features for each patch whose size is f . Each block includes a 1 Dimensional CNN (1D-CNN), 1D-Batch Normalization, 1D-Max pooling layer with a kernel size of 2 and a stride size of 2, and a Rectified Linear Unit activation function. The 1D-CNN hyperparameters differ based on dataset characteristics as shown in Table 4. Specifically, we adopt 2 CNN blocks for C-MAPSS due to the small patch sizes in this dataset. While for HAR and ISRUC-S3 with larger patch sizes, 3 CNN blocks are employed. An MLP follows the CNN blocks, mapping sensor features to a general feature space with an output hidden dimension of d_h . Subsequently, the learned sensor features of each patch are used for positional encoding, followed by subsequent graph construction. Here, as we separately process each sensor, the input dimension of CNN is 1.

For graph construction, we adopt trainable parameters $W_s \in \mathbb{R}^{d_h \times d_h}$ to improve the expressive capacity of the graph construction. In the GNN-based encoder, the updating stage is followed by the propagation stage to learn effective sensor features with trainable parameters $W_g \in \mathbb{R}^{d_h \times d_h}$. Additionally, moving windows are employed to capture local spatial-temporal dependencies within the graph, with a window size set to 2 based on prior studies [34]. After GNN, a function $f_l(\cdot)$ followed by the readout function is employed to learn final representations for downstream tasks. To accommodate diverse dataset properties, the configuration of $f_l(\cdot)$ is adjusted accordingly. The specific number of layers and hidden dimension are shown in Table 4.

Based on the above encoders, our methods are performed on an NVIDIA GeForce RTX 3080Ti GPU using PyTorch 1.9. We trained

the model with an ADAM optimizer over 50 epochs. The batch size varies across datasets, as shown in Table 4.

Received 20 February 2007; revised 12 March 2009; accepted 5 June 2009